Rich, A., Nordheim, A., & Azorin, F. (1983) *J. Biomol. Struct. Dyn. 1*, 1-19.
Rich, A., Nordheim, A., & Wang, A. H.-J. (1984) *Annu. Rev. Biochem. 53*, 791-846.
Romaniuk, P. J., & Eckstein, F. (1982) *J. Biol. Chem. 257*, 7684-7688.
Schaller, H., Weimann, G., Lerch, B., & Khorana, H. G. (1963) *J. Am. Chem. Soc. 85*, 3821-3827.
Soumpasis, D.-M. (1984) *Proc. Natl. Acad. Sci. U.S.A. 81*, 5116-5120.
Stec, W. J., Zon, G., & Egan, W. (1984) *J. Am. Chem. Soc. 106*, 6077-6078.
Still, W. C., Kahn, M., & Mitra, A. (1978) *J. Org. Chem. 43*, 2923-2925.
Thamann, T. J., Lord, R. C., Wang, A. H. T., & Rich, A. (1981) *Nucleic Acids Res. 9*, 5443-5457.
Thomas, G. A., & Peticolas, W. L. (1984) *Biochemistry 23*, 3202-3207.
van der Marel, G. A., Marugg, J. E., de Vroom, E., Wille, G., Tromp, M., van Boeckel, C. A. A., & van Boom, J. H. (1982) *Recl. Trav. Chim. Pays-Bas 101*, 234-241.
Wang, A. H.-J., Quigley, G. J., Kolpak, F. J., Crawford, J. L., van Boom, J. H., van der Marel, G., & Rich, A. (1979) *Nature (London) 282*, 680-686.
Wang, A. H.-J., Quigley, G. J., Kolpak, F. J., van der Marel, G., van Boom, J. H., & Rich, A. (1981) *Science (Washington, D.C.) 211*, 171-176.
Wang, A. H.-J., Hakoshima, T., van der Marel, G., van Boom, J. H., & Rich, A. (1984) *Cell (Cambridge, Mass.) 37*, 321-331.
Watson, J. D., & Crick, F. M. C. (1953) *Nature (London) 171*, 737-738.
Zarling, D. A., Arndt-Jovin, D. J., Robert-Nicoud, M., McIntosh, L. P., Thomae, R., & Jovin, T. M. (1984) *J. Mol. Biol. 176*, 369-415.

Axial Ligands of Chloroplast Cytochrome *b*-559: Identification and Requirement for a Heme-Cross-Linked Polypeptide Structure†

G. T. Babcock,*,‡ W. R. Widger,§ W. A. Cramer,*,§ W. A. Oertling,‡ and J. G. Metz‖,⊥

Department of Chemistry, Michigan State University, East Lansing, Michigan 48824-1322, Department of Biological Sciences, Purdue University, West Lafayette, Indiana 47907, and Department of Biological Sciences, University of Missouri, Columbia, Missouri 65211

Received December 31, 1984

ABSTRACT: Optical, resonance Raman, and electron paramagnetic resonance spectroscopies have been used to characterize the ligands and spin state of the chloroplast cytochrome *b*-559. The protein was isolated from both maize and spinach in a low-potential form. The spectroscopic data indicate that the heme iron in both ferric and ferrous cytochrome *b*-559 is in its low-spin state and ligated in its fifth and sixth coordination positions by histidine nitrogens. Electron paramagnetic resonance data for the purified spinach cytochrome are in good agreement with those determined by Bergström and Vänngård [Bergström, J., & Vänngård, T. (1982) *Biochim. Biophys. Acta 682*, 452-456] for a low-potential membrane-bound form of cytochrome *b*-559. The *g* values of high-potential cytochrome *b*-559 are shifted from those of its low-potential forms; this shift is interpreted as arising from a deviation of the planes of the two axial histidine imidazole rings from a parallel orientation. The model is consistent with the physical data and may also account for the facility with which cytochrome *b*-559 can be converted between low- and high-potential forms. Recent biochemical and molecular biological data [Widger, W. R., Cramer, W. A., Hermodson, M., Meyer, D., & Gullifor, M. (1984) *J. Biol. Chem. 259*, 3870-3876; Herrmann, R. G., Alt, J., Schiller, D., Cramer, W. A., & Widger, W. R. (1984) *FEBS Lett. 179*, 239-244] have shown that two polypeptides, one with 83 residues and a second with 39 residues, most likely constitute the protein portion of the cytochrome. Each of the polypeptides, however, contains only a single histidine. Thus, to provide the bis(histidine) axial ligation required by the physical data, we postulate that the heme acts as a cross-linker by coordinating histidines from two different polypeptide chains.

The chloroplast cytochrome *b*-559 is a membrane protein intrinsic to the core complex of photosystem II (PSII). Although this association and other data (Butler, 1978; Matsuda & Butler, 1983) provide circumstantial links between this protein and the water-splitting, oxygen-evolving function of PSII, elucidation of its function has proven difficult (Cramer et al., 1981). A 9-10-kilodalton (kDa)[1] polypeptide associated with this cytochrome was recently purified both from maize (Metz et al., 1983) and from spinach chloroplasts (Widger et al., 1984a). The purified cytochrome was used to determine

† This research was supported by National Institutes of Health Grant GM 25480 and the Photosynthesis Program of the Competitive Research Grants Office of the U.S. Department of Agriculture (to G.T.B. and W.A.O.) and by National Science Foundation Grant PCM-8403308 (to W.A.C. and W.R.W.). This paper is dedicated to the memory of Professor Warren L. Butler.

‡ Michigan State University.
§ Purdue University.
‖ University of Missouri.
⊥ Present address: Solar Energy Research Institute (SERI), Golden, CO 80401.

[1] Abbreviations: kDa, kilodalton(s); SDS, sodium dodecyl sulfate; Hepes, 4-(2-hydroxyethyl)-1-piperazineethanesulfonic acid; Tricine, *N*-[tris(hydroxymethyl)methyl]glycine; HPLC, high-performance liquid chromatography; PMSF, phenylmethanesulfonyl fluoride; Tris, tris(hydroxymethyl)aminomethane; EDTA, ethylenediaminetetraacetic acid; Chl, chlorophyll; EPR, electron paramagnetic resonance; LDS, lithium dodecyl sulfate.

0006-2960/85/0424-3638$01.50/0

the amino acid composition of the 9–10-kDa polypeptide as well as an N-terminal amino sequence of 27 residues (Widger et al., 1984a). This sequence, together with the antibody generated to HPLC-purified cytochrome polypeptide (Widger et al., 1984a), allowed location of the gene on the plastid chromosome of spinach (Westhoff et al., 1985) and determination of its complete nucleotide sequence and thereby the amino acid sequence of an 83 amino acid polypeptide (Herrmann et al., 1984). This sequence confirmed the amino acid composition data (Widger et al., 1984a) in showing the presence of one histidine residue in the 9-kDa polypeptide. The absence of lysine and internal methionine residues indicated that the His residue was the only commonly occurring heme ligand present in this polypeptide. The gene sequence also indicated the possibility that a second 39-residue polypeptide, again containing a single histidine residue, might be part of the cytochrome *b*-559 protein (Herrmann et al., 1984), and a small polypeptide of about this size was always seen in the gels of the purified protein (Metz et al., 1983; Widger et al., 1984a). Because neither polypeptide contained more than 1 histidine, and the 39-residue polypeptide 1 methionine, interest was focused on identifying the axial heme ligands of the cytochrome and on determining whether heme coordination requires more than 1 polypeptide. In the present experiments, we have used optical, resonance Raman, and electron paramagnetic resonance spectroscopic measurements to address this question with isolated cytochrome *b*-559. Our results support a structure for cytochrome *b*-559 in which both the fifth and sixth ligands to the heme iron are histidine nitrogens. This observation indicates that at least two polypeptides per heme unit are required in the assembly of the holoprotein.

Experimental Procedures

Purification of Cytochrome b-559 from Spinach Chloroplasts. Most of the experiments in the present work were carried out with the spinach cytochrome (Widger et al., 1984a). The entire procedure was performed in the presence of the protease inhibitors PMSF (0.5 mM), benzamidine (2 mM), and ϵ-aminocaproic acid (2 mM). The inhibitor Trasylol was added to the membrane solubilization medium at 50 units/mL. Chloroplasts with unstacked lamellae were isolated in 0.4 M sucrose and 50 mM Tris, pH 8.0, and were washed in 10 mM Tris–Tricine and 5 mM EDTA, pH 7.8. The chloroplasts were extracted 3 times with ethanol to remove the chlorophyll. The membranes were washed once in 50 mM Hepes, pH 6.8, and then in 50 mM Hepes and 0.5% Triton X-100, pH 6.8.

The three cytochromes, *f*, b_6, and *b*-559, were solubilized by extracting the membranes at a final concentration equivalent to 2.5 mg of Chl/mL before extraction in 2% Triton X-100, 4 M urea, and 0.15 M Hepes, pH 6.8. The initial addition was 4% Triton, 0.3 M Hepes, and protease inhibitors at twice the final concentration. Eight molar urea was then added in an equal volume to obtain the final concentration of 4 M and then stirred at 0 °C for 15–20 min. The amount of *b*-559 solubilized is approximately 1 heme:400 chlorophylls, about 80% of the total cytochrome *b*-559 heme in these membranes. After centrifugation at 25000*g* for 20 min, the supernatant was collected, assayed for cytochrome content, and placed on a DEAE-cellulose (DE52) column equilibrated in 2% Triton X-100, 2 M urea, and 0.1 M Hepes, pH 6.8. The cytochromes were eluted in the first green fraction. The eluant from the DE52 column was placed on a small hydroxylapatite column, equilibrated in the same buffer, that removed almost all of the cytochrome *f* while allowing the *b*-559 and *b*-563 to pass through. This eluant was dialyzed overnight against 50 volumes of 20 mM Tricine, pH 8.0, and loaded on the second DEAE column (DEAE-Sephacel) equilibrated in 20 mM Tricine, pH 8.0. The *b*-559 and a small amount of residual cytochrome *f* bound to the column, which was then developed by consecutive washing with the following buffers: (i) 2% Triton X-100, 2 M urea, and 0.1 M Hepes, pH 6.8, to remove *b*-563 and other contaminants; (ii) 20 mM Tricine, pH 8.0, to remove detergent and urea from the column; (iii) 20 mM Tricine and 0.5 M KCl, pH 8.0, to remove the cytochrome *f* and other contaminants; and (iv) 1% octyl glucoside, 2 M urea, 0.1 M Hepes, and 0.5 M KCl, pH 6.8, to elute the cytochrome *b*-559. The cytochrome *b*-559 was concentrated by using a membrane with a 75000 molecular weight cutoff that retained the aggregated or oligomeric (M_r >100000) *b*-559 lipoprotein, and the precipitated cytochrome was gently solubilized in 1% octyl glucoside and 50 mM Tricine, pH 8.0. Any precipitate that did not dissolve was removed by centrifugation and discarded. The procedure resulted in a yield of approximately 30–50% of the starting material, 6–10 mg of purified *b*-559 from starting material containing 600 mg of chlorophyll.

Cytochrome *b*-559 from maize was isolated as described by Metz et al. (1983) except that washed thylakoid membranes were used as the starting material instead of PSII particles.

Protein and Chlorophyll Estimation. Protein was estimated by the method of Lowry et al. (1951) and chlorophyll by the method of Arnon (1949). Pyridine hemochromagen spectra were recorded by using the method of Rieske (1967).

Spectrophotometry. Absorbance difference spectra of cytochrome extracts and of the purified cytochrome in the 695-nm region were measured by using a Kontron UVIKON-810 dual-beam spectrophotometer using packaged peak detection routines. Dithionite-reduced minus ferricyanide-oxidized spectra or the individual component spectra were typically recorded at scan rates of 20–50 nm/min. The optical spectra shown in Figure 4 were recorded by using a Perkin-Elmer Lambda 5 spectrophotometer.

Electron Paramagnetic Resonance. EPR measurements were carried out by using a Bruker ER200D spectrometer. An Oxford ESR-9 liquid helium cryostat was used to maintain sample temperature; frequencies were measured with a Hewlett-Packard frequency counter, and magnetic fields were determined with a Bruker gaussmeter accessory. The *g* values quoted in Table I were determined by recording the EPR spectrum of the species of interest and then returning to measure accurately both the magnetic field and the frequency at the extrema and zero-crossing in the spectrum.

Raman Spectroscopy. Resonance Raman spectroscopy for cytochrome *b*-559 and its model compounds was carried out by using laser lines in resonance with the Soret optical transitions and the instrumentation described by Callahan & Babcock (1981). Sample temperature was maintained by flowing cold N_2 gas through the Raman cuvette holder; the temperature was monitored with a thermocouple in contact with the cuvette. Optical spectra were recorded before and after Raman measurements in order to assess sample stability.

Materials. Dithiothreitol, LDS, phenylmethanesulfonyl fluoride, benzamidine, ϵ-aminocaproic acid, iron(3+) protoporphyrin IX, EDTA, Tris, Tricine, and Triton X-100 were purchased from Sigma; Trasylol was from Mobay Chemicals (FBS Pharmaceuticals, New York). Hepes was obtained from Research Organics, cellulose powder and DE52 were from Whatman, octylglucoside was from Calbiochem, Sephacel was from Pharmacia, and all other chemicals were of the highest commercial quality available.

Table I: g Values and Ligand Field Parameters for Various Low-Spin Ferric Heme Species

compd	g_z	g_y	g_x	tetragonality[a]	rhombicity[a]	tetragonality[b]	rhombicity[b]
cyt b-559							
maize[c] (isolated)	2.94	2.27	1.54	1.92	0.57	2.41	0.77
spinach[c] (isolated)	2.93	2.26	1.55	1.94	0.56	2.49	0.78
high potential[d] (membrane)	3.08	2.16	1.36[e]	1.52	0.41	2.55	0.91
low potential[d] (membrane)	2.94	2.26	1.50[e]	1.86	0.58	2.30	0.76
cyt b_5[f]	3.05	2.22	1.41	1.62	0.50	2.42	0.86
Fe^{3+}PPIX(N-MeIm)$_2$[c] (neutral)	2.95	2.26	1.52	1.87	0.56	2.41	0.78
Fe^{3+}PPIX(N-MeIm)$_2$[c] (alkaline)	2.74	2.27	1.72	2.80	0.67	2.75	0.70
cyt c[g]	3.06	2.24	1.24	1.46	0.57	1.83	0.77
cyt c[h] (alkaline) His-Fe-NH_2	3.35	2.06	1.50	1.39	0.25	4.87	1.27

[a] Taylor (1977) axis system, summarized in Palmer (1985). [b] Blumberg & Peisach (1971) axis system. [c] This work. [d] Bergström & Vänngård (1982). [e] Calculated by assuming no covalency (i.e., that $g_{xx}^2 + g_{yy}^2 + g_{zz}^2 = 16$); see Taylor (1977). [f] Ikeda et al. (1974). [g] Salmeen & Palmer (1968). [h] Brautigan et al. (1977).

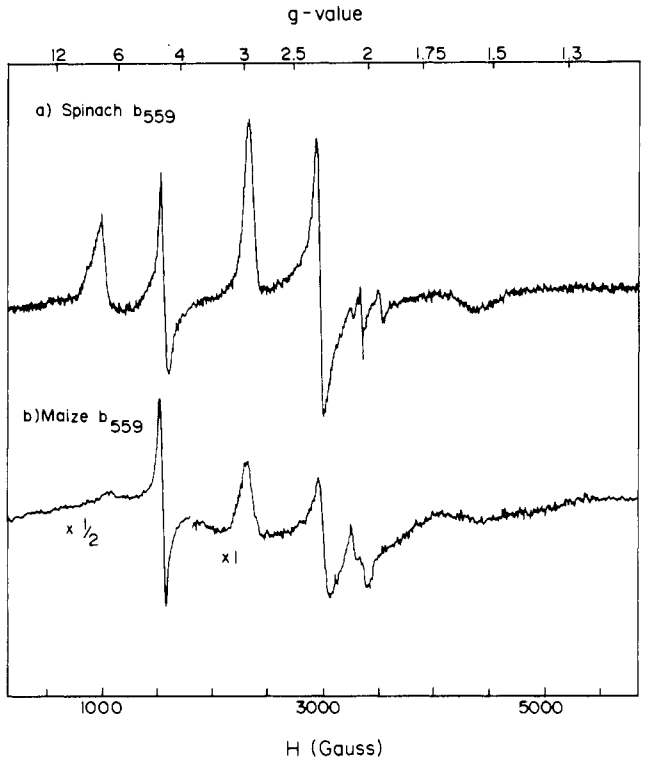

FIGURE 1: EPR spectra of isolated spinach (a) and maize (b) cytochrome b-559. The spinach cytochrome was dissolved in 1% octyl glucoside and 50 mM Hepes, pH 7.0, at a concentration of ~100 μM; the maize protein was dissolved in 50 mM Tris, pH 8.0, and 0.2% Triton X-100 at a concentration of ~40 μM. For the spinach protein, the following conditions were used: microwave power, 5 mW; modulation amplitude, 20 G; time constant, 0.1 s; sweep time, 200 s; gain, 8×10^5; temperature, 10 K; the spectrum was obtained as a single scan. For maize cytochrome b-559, the conditions were the following: microwave power, 6.3 mW; modulation amplitude, 20 G; time constant, 0.1 s; sweep time, 200 s; gain, 1×10^6; temperature, 8.2 K; the spectrum was obtained as the average of four scans.

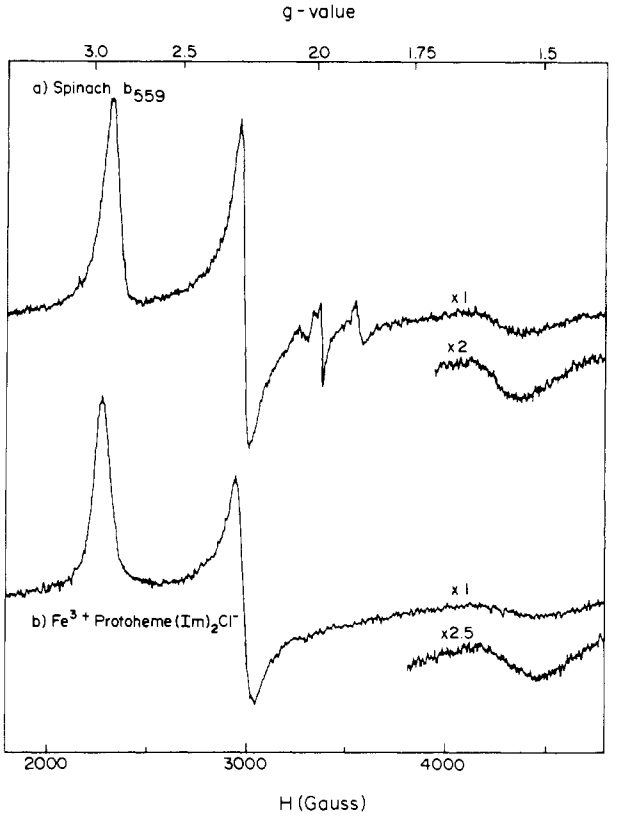

FIGURE 2: EPR spectra of spinach cytochrome b-559 (a) and bis(N-methylimidazole)iron(3+) protoheme chloride (b). The cytochrome was in the same buffer as described for Figure 1; for the model compound, iron(3+) protoheme chloride was dissolved in a buffer which contained 0.1 M phosphate, 0.7 M N-methylimidazole, and 0.07 M cetyltetramethylammonium bromide at pH 7.4. The EPR spectrum of the model is independent of pH in the neutral pH range (pH 6–8). The concentration of both the protein and the model was ~100 μM. Instrumental conditions as described in Figure 1a were used in recording both spectra.

RESULTS

EPR Spectroscopy. Figure 1a shows a wide-field EPR spectrum of purified spinach cytochrome b-559 at 10 K. Although there are signals in the $g = 6$, $g = 4.3$, and $g = 2$ regions, indicative of heme-bound high-spin iron, rhombic iron, and free radicals, respectively, the major paramagnet (>95%) in this sample is the low-spin species with g values in the 3.0, 2.3, and 1.5 range. Figure 1b shows the corresponding wide-field EPR spectrum for cytochrome b-559 isolated from maize. For this preparation, the $g = 4.3$ signal is somewhat more prominent than that in the spinach protein, and the high-spin ($g = 6$) signal has decreased considerably. Again, the major species is the low-spin form with g values in the 3, 2.3, and 1.5 range. As the major cytochrome b-559 component in chloroplast fragments is also low spin (Bergström & Vänngård, 1982), these spectra demonstrate that the isolation procedure does not alter the heme iron spin state in either spinach or maize.

Blumberg & Peisach (1971) have shown that in many cases low-spin heme iron axial ligands can be identified provided all three g values are known. These are established for isolated spinach cytochrome b-559 in Figure 2a, where we present higher resolution EPR spectra for this species. The g values determined from this spectrum and the corresponding ligand field parameters [tetragonality (V/λ) and rhombicity ($|V/\Delta|$)] are summarized in Table I, along with the corresponding values for the maize protein. The ligand field parameters were

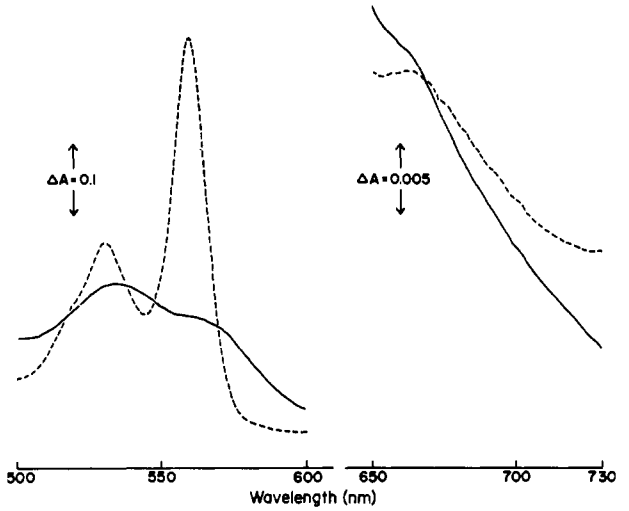

FIGURE 3: Comparison of the visible light absorbance properties of cytochrome *b*-559 in the α (left) and 695-nm regions (right); oxidized (---) by ferricyanide and reduced (—) by dithionite. The cytochrome was dissolved in a buffer which contained 1% octyl glucoside and 50 mM Hepes, pH 7.0, at a concentration of 22 μM.

calculated according to the formalism given by Taylor (1977) but with the original axis system defined by Blumberg & Peisach (1971) to facilitate comparison with their tabulated data. Also included in Table I are the rhombicity and tetragonality parameters in Taylor's (correct) axis system (see below). The *g* values and the ligand field parameters are characteristic of bis(histidine) axial ligation (Blumberg & Peisach, 1971; Palmer, 1985), and in Figure 2b, we show the spectrum of the bis(*N*-methylimidazole)iron(3+) protoporphyrin IX at neutral pH for direct comparison. The spectrum was recorded under the same experimental conditions as were used for the isolated proteins; the *g* values and ligand field parameters are given in Table I. These confirm the close similarity in magnetic resonance parameters for the purified maize and spinach *b*-559 proteins and the model compound. For example, purified spinach cytochrome *b*-559 has *g* values of 2.93, 2.26, and 1.55, and the bis(*N*-methylimidazole) ferric protoheme model has *g* values of 2.95, 2.26, and 1.52. To demonstrate the sensitivity of the EPR spectrum to the nature of the axial ligands, *g* values and ligand field parameters for several other heme proteins and model compounds are also given in Table I [see also Palmer (1985); a comprehensive experimental study of the relationship between axial ligands and *g* values/ligand field parameters for low-spin ferric iron porphyrins has recently appeared (Walker et al., 1984)].

Optical Spectroscopic Measurement at 695 nm. The EPR data above indicate bis(histidine) axial ligation in isolated, low-potential cytochrome *b*-559. Because of the occurrence of a methionine residue in the smaller polypeptide (see above), however, it is necessary to exclude further the possibility that methionine sulfur coordinates the heme iron. To this end, the optical absorption of the purified spinach cytochrome was measured in the oxidized state at 695 nm, where there is an absorption band associated with methionine–heme coordination that is seen in high-potential *c*-type cytochromes (Schechter & Saludjian, 1967; Smith & Williams, 1970). The extinction coefficient of this band, $\sim$800 M^{-1} cm^{-1}, is approximately $^1/_{20}$th that of the reduced–oxidized α-band. Examination of the absorbance properties of spinach cytochrome *b*-559 in the 695-nm region, at a 20-fold scale expansion relative to the α-band, shows the absence of any 695-nm band at an instrument sensitivity setting that would have allowed detection at a level $^1/_{200}$th that measured for the α-band (Figure 3). A small absorbance change is seen near 665 nm that is affected by dithionite reduction and appears to result, as determined by fluorescence emission and excitation spectra (not shown), from a small amount of chlorophyll present in the preparation.

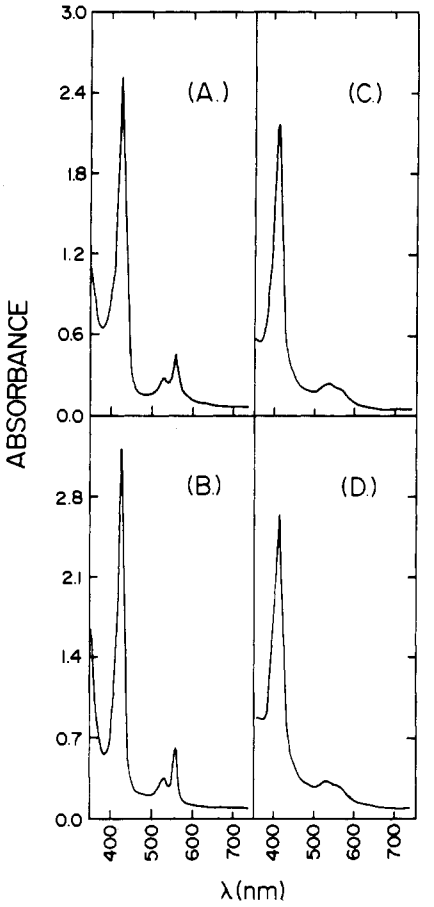

FIGURE 4: Visible and near-UV optical absorption spectra of cytochrome *b*-559, oxidized (D) and reduced (B), and of bis(*N*-methylimidazole)iron protoheme, oxidized (C) and reduced (A). The cytochrome was dissolved in 50 mM Hepes buffer which contained 2% octyl glucoside at pH 7.0. Protoheme chloride was dissolved in the same buffer described in Figure 2. Reduction was carried out by using solid dithionite. The optical path length was 0.5 cm, and the temperature was 25 °C. The same samples were used for the resonance Raman experiments of Figures 5 and 6.

Table II: Absorption Maxima for Cytochrome *b*-559 and Bis(imidazole) Protoheme

	Soret (nm)	visible (nm)
cyt *b*-559 (ox)	413	534 (br), 562 (br)
Fe^{3+}(PPIX)$(Im)_2Cl^-$	413	535, 564
cyt *b*-559 (red)	427	530, 559
Fe^{2+}(PPIX)$(Im)_2$	426	530, 559

Optical and Raman Spectroscopy. In terms of EPR properties, the data above show that bis(*N*-methylimidazole) protoheme is a good model for cytochrome *b*-559. We tested this structural assignment in more detail and also investigated the reduced protein by recording optical and Soret excitation Raman spectra for the isolated spinach protein and bis(*N*-methylimidazole) protoheme models in ferric and ferrous oxidation states. Figure 4 shows a comparison of the optical data. The absorption maxima in the visible and Soret regions for the various species are summarized in Table II; good agreement between the protein and the model compound data is apparent.

Empirical correlations have been developed over the past decade which relate the frequencies of several iron porphyrin

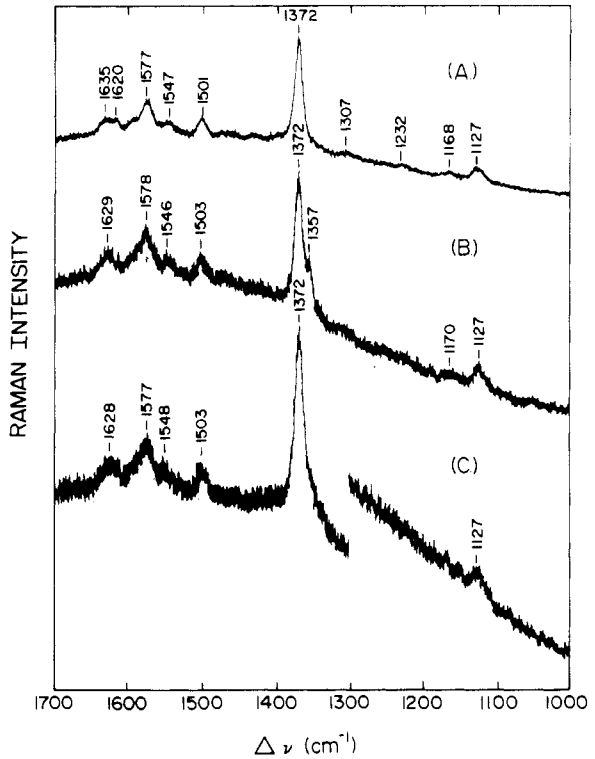

FIGURE 5: Resonance Raman spectra in the high-frequency region for bis(*N*-methylimidazole)iron(3+) protoheme (A) and oxidized cytochrome *b*-559 (B and C). The buffers and concentrations were as in Figure 4. Laser excitation was at 413.1 nm at a power of ~20 mW; the sample temperature was maintained at 5 °C. In (B), photoreduction of the static cytochrome *b*-559 sample is apparent as the 1357-cm^{-1} shoulder on ν_4, the oxidation-state marker. Photoreduction is minimized by flowing the sample (C).

vibrations to the coordination geometry, spin state, and pattern of peripheral substitution of the heme chromophore (Spaulding et al., 1975; Spiro et al., 1979; Callahan & Babcock, 1981). As a consequence, resonance Raman spectroscopy has become a useful analytical technique in characterizing the local environment around the redox center in heme proteins. The Raman spectra (1000–1700-cm^{-1} region) for bis(*N*-methylimidazole) ferric protoheme and for ferric cytochrome *b*-559 are shown in Figure 5. We also recorded the low-frequency Raman spectra (200–1000 cm^{-1}) of these species (not shown); the principal vibrations observed in both frequency regions are collected in Table III and assigned according to analyses carried out by Abe et al. (1978), Callahan & Babcock (1981), and Choi et al. (1982). For the protein, we observed photoreduction of the heme chromophore for static samples maintained at 6 °C under 15 mW of laser illumination. This is apparent in Figure 5B as the shoulder at 1358 cm^{-1}. By flowing the sample and maintaining an O_2 atmosphere above the reservoir, we were able to record Raman spectra of the oxidized species in which the effects of photoreduction were minimized (Figure 5C). Good agreement between the protein and model compound data is observed. The appearance of $\bar{\nu}_3$ at 1503 cm^{-1} in the protein (1501 cm^{-1} in the model) establishes the 6-coordinate, low-spin nature of the heme iron, and as expected for a protoheme species with this geometry, the polarized mode, $\bar{\nu}_2$, is observed at 1577 cm^{-1}. The 1628-cm^{-1} mode in the protein is assigned as arising from a coalescence of $\bar{\nu}_{10}$, expected at 1638 cm^{-1} for the 6-coordinate, low-spin state, and the C=C stretching mode of the peripheral vinyls at ~1622 cm^{-1} (Choi et al., 1982). The frequency observed for $\bar{\nu}_{38}$, 1548 cm^{-1}, is consistent with the conclusions above.

Table III: Principal Vibrational Frequencies (cm^{-1}) for Cytochrome *b*-559 and Bis(imidazole) Protoheme

cyt *b*-559 (ox)	bis(*N*-methylimidazole)iron(3+) protoheme	cyt *b*-559 (red)	bis(*N*-methylimidazole)iron(2+) protoheme	assignment mode no.[a] (symmetry)
344	346	349	345	
377	384	385	384	
419	420	418	414	
676	676	675	674	
744	744	744	744	
		1002	966	ν_{45} (E_u)
		1125	1116	ν_{22} (A_{2g})
1127	1127		1130	$\nu_6 + \nu_8$ (A_{1g})
1170	1168	1168	1171	ν_{30} (B_{2g})
	1232	1222	1223	ν_{13} (B_{1g})
	1307	1302	1306	ν_{21} (A_{2g})
1372	1372	1355	1356	ν_4 (A_{1g})
		1386	1389	ν_{20} (A_{2g})
		1424	1424	δ_s (=CH_2)
			1467	ν_{28} (B_{2g})
1503	1501	1488		ν_3 (A_{1g})
		1532		ν_{11} (B_{1g})
1548	1547	1554	1555	ν_{38} (E_u)
1577	1577	1579	1578	ν_2 (A_{1g})
		1600	1600	ν_{37} (E_u)
1628	1620	1616	1616	ν (C=C)
	1635			ν_{10} (B_{1g})

[a] Mode numbering from Abe et al. (1978); assignments from Callahan & Babcock (1981) and from Choi et al. (1982).

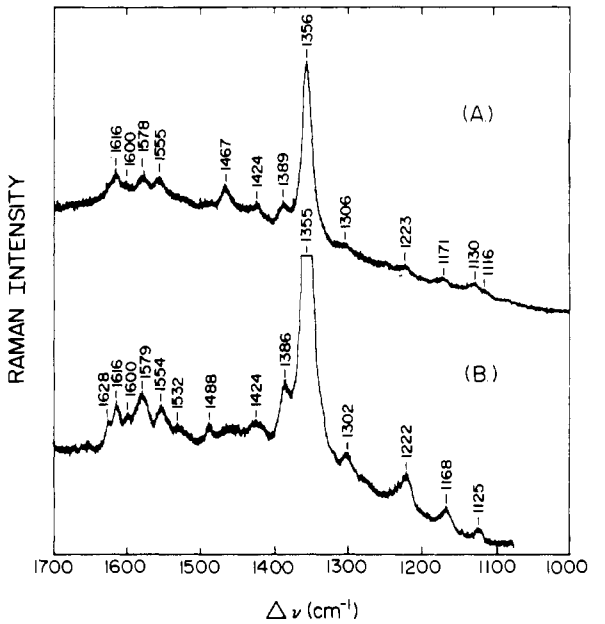

FIGURE 6: Resonance Raman spectra in the high-frequency region for bis(*N*-methylimidazole)iron(2+) protoheme (A) and reduced cytochrome *b*-559 (B). Buffers, concentrations, and instrument conditions as in Figure 5. The Raman spectrum of the model is less resolved than that of the protein owing to the lower protoheme concentration in the model compound solution (see Figure 4).

The Raman spectra for the reduced, bis(*N*-methylimidazole) protoheme model compound and the reduced cytochrome *b*-559 are shown in Figure 6A,B. The principal frequencies observed in these spectra as well as in analogous low-frequency spectra (not shown) are also collected and assigned in Table III. Good agreement in the frequencies observed for $\bar{\nu}_{38}$, $\bar{\nu}_2$, $\bar{\nu}_{37}$, and $\bar{\nu}_{10} + \bar{\nu}_{C=C}$ is observed between the two sets of data. In the protein, $\bar{\nu}_3$ is clearly observed at 1488 cm^{-1} and is assigned in analogy with $\bar{\nu}_3$ as reported by Choi et al. (1982) for the ferrous protoheme model even though this mode is not obvious in the model spectrum in Figure 6A. Conversely, $\bar{\nu}_{28}$

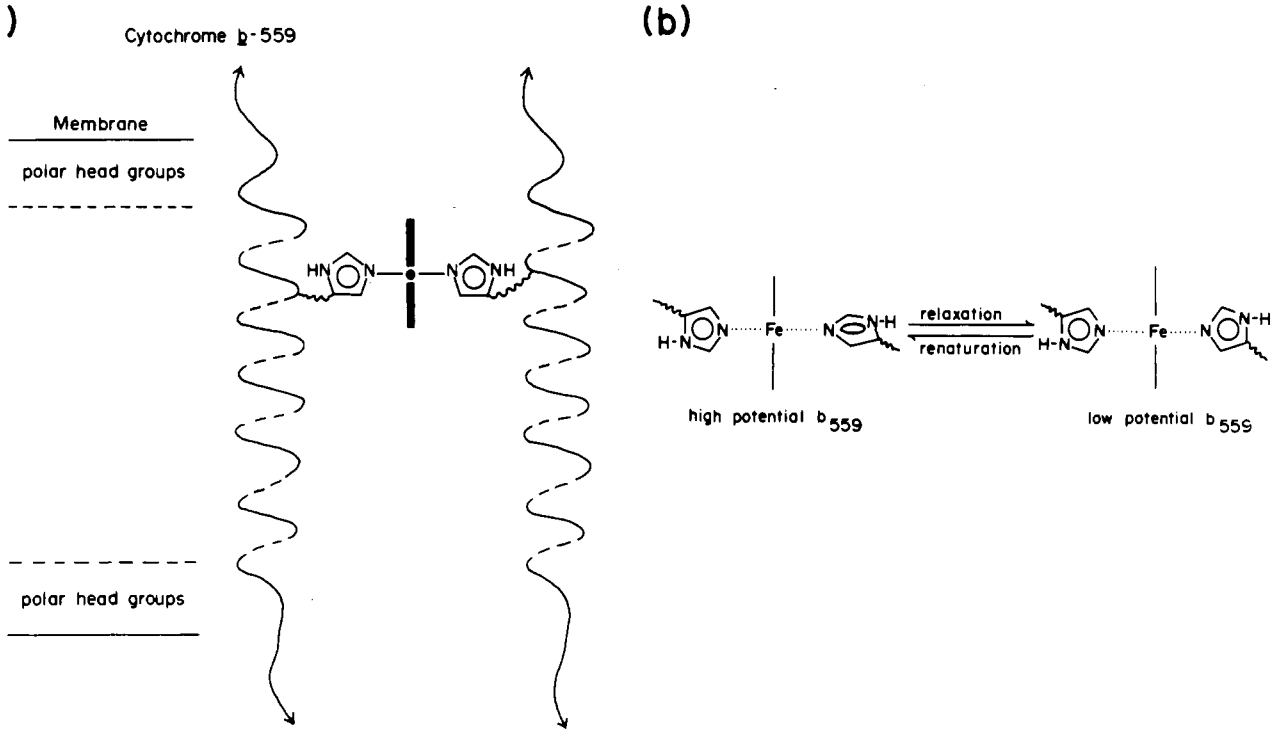

FIGURE 7: (a) Model for the protein binding site for protoheme in cytochrome *b*-559. (b) Model for the orientation of the two histidine imidazole rings in cytochrome *b*-559. In the low-potential form, the planes of the imidazoles are postulated to be parallel; in the high-potential form, the plane of one of the two rings is rotated so that a parallel orientation of the two ring planes does not occur.

at 1467 cm^{-1} is observed in the model spectrum although it appears only weakly, if at all, in the protein spectrum. The vinyl scissors model (δ_S =CH_2) is observed at 1424 cm^{-1} in both model and protein and supports the conclusions reached above that these peripheral groups are unmodified in the protein in both its oxidized and its reduced states. In the frequency region below 1300 cm^{-1}, the correspondence between ferrous *b*-559 and the ferrous protoheme model is good.

Discussion

The spectroscopic results presented above indicate strongly that the imidazole side chains of histidine occupy the fifth and sixth coordination positions of the protoheme iron of cytochrome *b*-559 in its isolated, low-potential form. Moreover, the heme iron is predominantly in its low-spin state in both its ferric and its ferrous valence states. While this result is not unexpected given the common occurrence of bis(histidine) ligation in *b*-type cytochromes and the results of previous spectroscopic characterization of cytochrome *b*-559 [e.g., see Bergström & Vänngård (1982)], the conclusion has interesting ramifications in view of recent amino acid analysis and sequence data (Widger et al., 1984a; Herrmann et al., 1984) for cytochrome *b*-559. Two polypeptides, one with 83 residues and a second with 39 residues, apparently constitute the protein component of cytochrome *b*-559. The 83-residue polypeptide was identified by antibody, and a 39-residue species is coded by a contiguous gene. Sequence data show that each of these polypeptides has only a single histidine and that this residue occurs on the N-terminal side of a 25–26-residue hydrophobic domain. Therefore, to account for both the spectroscopic data presented above which identify bis(histidine) axial ligation and the amino acid analysis and sequence data which show only a single histidine per polypeptide, the heme binding unit must consist of two polypeptides bridged by the ligated protoheme chromophore. The structure we propose is shown schematically in Figure 7a. At present, it is unclear whether the two polypeptides involved in the structure are both 83-residue polypeptides, both 39-residue polypeptides, or one of each [see also Herrmann et al. (1984)]. These different possibilities arise, and further implicate involvement of the 39-residue polypeptides, because of the similar location of the histidine in the sequence of each of the two polypeptides, i.e., on the N-terminal side of what appears to be a hydrophobic, membrane-spanning domain. Thus, all three models for the polypeptide components of the heme binding domain (i.e., 83–83, 39–39, or mixed 39–83) predict the perpendicular orientation of the protoheme of cytochrome *b*-559 with respect to the membrane shown in Figure 7a. This assignment of orientation is consistent with the EPR data of Bergström & Vänngård (1982) on oriented chloroplast membranes which indicate that the heme normal is in the membrane plane. Biochemical proof for the participation of the 39 amino acid polypeptide in the cytochrome *b*-559 protein awaits N-terminal sequencing of a component of about this size and approximately the correct amino acid composition that is seen on SDS gels (W. R. Widger and W. A. Cramer, unpublished results).

If a stoichiometry of two *b*-559 hemes per P680 reaction center in chloroplasts (Cramer et al., 1981) is taken into account, four polypeptides organized as two dimers or a tetramer are needed for coordination of the two hemes. The relevance of such a structure to oxygen evolution, however, is uncertain because the *b*-559/P680 stoichiometry appears to be only one in highly active, oxygen-evolving PSII particles isolated from spinach [e.g., see Ghanotakis et al. (1984)].

The model of Figure 7a suggests a mechanism by which the well-known lability of the *b*-559 redox potential (Cramer & Whitmarsh, 1977) and in vivo *g* values can be rationalized. In its membrane environment, cytochrome *b*-559 can exist in a high-potential form ($\epsilon_m' \simeq 400$ mV) or in a variety of low-potential forms which appear to have $\epsilon_m \simeq 0$ mV as a lower bound. Corresponding to this thermodynamic variation is a structural variation which manifests itself as a midpoint potential dependence in the g_z and g_y values of the cytochrome. High-potential *b*-559 has $g_z = 3.08$ and $g_y = 2.16$, whereas

the lower potential forms of the membrane-bound cytochrome have $g_z = 2.94$ and $g_y = 2.26$ (Bergström & Vänngård, 1982). Consistent with its EPR properties, purified *b*-559 is also a low-potential form of the protein (Cramer & Whitmarsh, 1977).

The data in Table I show that low-potential *b*-559, both in its purified and in its membrane-bound forms, has EPR parameters essentially identical with those of the bis(*N*-methylimidazole) protoheme model compound. As the geometery of the axial imidazoles in model compounds has been shown to influence the *g* values and ligand field parameters in bis(imidazole)-ligated heme species (Carter et al., 1981; Walker et al., 1984), the similar EPR properties for the model compound and low-potential *b*-559 indicate a similar geometry for the imidazole rings about the protoheme moiety in these two classes of compounds. High-potential *b*-559, on the other hand, exhibits a significant variation in its *g* values relative to those of the model compound. His–Met or His–Lys axial coordination as the source of this divergence is improbable, as shown above and by the absence of lysine in the sequence of the 83- and 39-residue polypeptides. The geometry of the axial histidines then appears to be a more likely source for the altered *g* values in high-potential *b*-559. We suggest that the physiologically relevant form of the protein has an unusual, strained configuation of the two axial histidines about the protoheme moiety. A similar situation apparently exists for the *b*-type cytochromes of the mitochondrial bc_1 and of the chloroplast b_6f complexes. These species exhibit g_z values in the 3.1–3.8 range but, nonetheless, appear to have bis(histidine) axial ligation (Salerno, 1984; Widger et al., 1984b). Palmer and co-workers (Carter et al., 1981; Palmer, 1985), Salerno (1984), and Walker et al. (1984) have considered the origin of such *g* shifts within the context of bis(histidine) ligation, and the following hypothesis has emerged (Palmer, 1985). For model compounds in which the planes of the axial imidazole rings are parallel to each other [e.g., bis(*N*-methylimidazole)iron(3+) protoheme], there is a large differential effect on the energies of the iron d_{xz} and d_{yz} orbitals (i.e., the ligand field splitting between these two orbitals becomes large). The EPR spectrum has values for g_z, g_y, and g_x in the 2.95, 2.25, and 1.55 range, and the rhombicity parameter in Taylor's axis system (1977) is in the 0.55–0.60 range, close to the maximum possible rhombicity of 0.67. For model compounds in which the planes of the axial imidazole rings become perpendicular to each other, the differential effect on d_{xz} and d_{yz} decreases, and the ligand field splitting between these orbitals becomes small. In the EPR spectrum, g_z increases to values above 3 while g_y and g_x decrease accordingly [if no covalency occurs, the sum, $g_z^2 + g_y^2 + g_x^2$, should equal 16 for low-spin ferric hemes (Taylor, 1977)]; the rhombicity parameter decreases relative to that observed in models in which a parallel plane geometry occurs for the imidazole ligands.

The EPR parameters for isolated and membrane-bound cytochrome *b*-559 can be interpreted within this model. Isolated maize and spinach *b*-559 have *g* and rhombicity values close to those of the bis(*N*-methylimidazole) protoheme model compound. This indicates that the planes of the two axial histidine imidazole rings, like those of the model, are close to being parallel. For high-potential membrane-bound *b*-559 only g_z and g_y have been measured (Bergström & Vänngård, 1982), but they show an increase in g_z and a decrease in g_y relative to the model compound, which is characteristic of a deviation from parallel alignment of the imidazole planes. To test this idea further, we have taken the g_z and g_y values of Bergström and Vänngård for membrane-bound high- and low-potential *b*-559 and calculated g_x values by assuming that no covalency occurs (Table I). From these *g* values, we determined ligand field parameters in both the Blumberg & Peisach (1971) axis system and the Taylor (1977) axis system. These values are given in Table I. The low-potential species has a rhombicity parameter (0.58) and *g* values similar to the parallel plane geometry model whereas the high-potential form, as suggested by the analysis above, has a significantly smaller rhombicity (0.41 in Taylor's correct axis system) indicative of a nonparallel imidazole plane orientation.

The conclusions from this analysis are shown in Figure 7b. Both low-potential *b*-559 and high-potential *b*-559 are envisioned as having bis(histidine) axial ligation. For the low-potential form, the planes of the two imidazoles are parallel, whereas in the high-potential form a more perpendicular alignment of the imidazoles occurs. The model is attractive in that it rationalizes the *g*-value difference between high- and low-potential *b*-559 in terms of structure. Moreover, it may also provide an explanation for the facility with which high-potential *b*-559 can be converted to the low-potential form (Cramer & Whitmarsh, 1977) and for the fact that the low-potential *b*-559 can be restored to its high-potential state in PSII particles by treatments which alter the state of the membrane, for example, by lipid addition (Matsuda & Butler, 1983). For an interesting hypothesis regarding the interplay between heme axial ligand stereochemistry and heme iron redox potential, see Korszun et al. (1985).

The absolute value of ϵ_m in *b*-type cytochromes must be determined by several effects in addition to the relative orientation of the imidazole planes. The mitochondrial cytochrome *b* and the chloroplast cytochrome b_6, both of which are likely to have bis(histidine) coordination, have high g_z values (Carter et al., 1981; Salerno, 1984; Palmer, 1985) but do not have anomalously positive midpoint potentials. However, like cytochrome *b*-559, these cytochromes also show a large decrease in the ϵ_m values upon solubilization from, or perturbation of, the membrane (Goldberger et al., 1962; Deeb & Hager, 1964; Böhme & Cramer, 1973). Thus, for these systems, the ϵ_m value may reflect the interplay between heme imidazole ligand orientation and other factors, such as dipole orientation or solvent accessibility, in the heme pocket. Depending on the relative contributions of these effects, the ϵ_m of the cytochrome may be anomalously positive, as in the case of *b*-559, or lower and more typical of that expected of *b*-type cytochromes, as in the case of mitochondrial *b* or chloroplast b_6.

ACKNOWLEDGMENTS

Several helpful discussions with Prof. G. Palmer on the relationship between heme ligand geometry and *g* values are acknowledged. We thank Lucy Winchester and Margy Lynch for help in the preparation of the manuscript.

Registry No. Fe^{3+}PPIX(*N*-Me-Im)$_2$, 78261-95-7; Fe, 7439-89-6; histidine, 71-00-1; nitrogen, 7727-37-9; heme, 14875-96-8; cytochrome *b*-559, 9044-61-5.

REFERENCES

Abe, M., Kitagawa, T., & Kyogoku, Y. (1978) *J. Chem. Phys. 69*, 4526–4534.

Arnon, D. I. (1949) *Plant Physiol. 24*, 1–5.

Bergström, J., & Vänngård, T. (1982) *Biochim. Biophys. Acta 682*, 452–456.

Blumberg, W. D., & Peisach, J. (1971) *Adv. Chem. Ser. No. 100*, 271–291.

Böhme, H., & Cramer, W. A. (1973) *Biochim. Biophys. Acta 325*, 275–283.
Brautigan, D. L., Feinberg, B. A., Hoffman, B. M., Margoliash, E., Peisach, J., & Blumberg, W. E. (1977) *J. Biol. Chem. 252*, 574–582.
Butler, W. L. (1978) *FEBS Lett. 95*, 19–25.
Callahan, P. M., & Babcock, G. T. (1981) *Biochemistry 20*, 952–958.
Carter, K., Tsai, A. L., & Palmer, G. (1981) *FEBS Lett. 132*, 243–246.
Choi, S., Spiro, T. G., Langtry, K. C., Smith, K. M., Budd, D. L., & La Mar, G. N. (1982) *J. Am. Chem. Soc. 104*, 4345–4351.
Cramer, W. A., & Whitmarsh, J. (1977) *Annu. Rev. Plant Physiol. 28*, 133–172.
Cramer, W. A., Whitmarsh, J., & Widger, W. R. (1981) in *Photosynthesis, Electron Transport and Phosphorylation* (Akogunoglou, G., Ed.) pp 509–521, Balaban International Science Services, Philadelphia, PA.
Deeb, S. S., & Hager, L. P. (1964) *J. Biol. Chem. 239*, 1024–1031.
Ghanotakis, D. F., Babcock, G. T., & Yocum, C. F. (1984) *Biochim. Biophys. Acta 765*, 388–398.
Goldberger, R., Pumphrey, A., & Smith, A. (1962) *Biochim. Biophys. Acta 58*, 307–313.
Herrmann, R. G., Alt, J., Schiller, D., Cramer, W. A., & Widger, W. R. (1984) *FEBS Lett. 179*, 239–244.
Ikeda, M., Lizuka, T., Takao, H., & Hagihara, B. (1974) *Biochim. Biophys. Acta 336*, 15–24.
Korszun, Z. R., Moffat, K., & Cusanovich, M. A. (1985) *Biophys. J.* (submitted for publication).
Lowry, O. H., Rosebrough, J. J., Farr, A. L., & Randall, R. J. (1951) *J. Biol. Chem. 193*, 265–275.
Matsuda, H., & Butler, W. L. (1983) *Biochim. Biophys. Acta 725*, 320–324.
Metz, J. G., Ulmer, G., Bricker, T. M., & Miles, D. (1983) *Biochim. Biophys. Acta 725*, 203–209.
Palmer, G. (1985) *Biochem. Soc. Trans.* (in press).
Rieske, J. S. (1967) *Methods Enzymol. 10*, 488–493.
Salerno, J. C. (1984) *J. Biol. Chem. 259*, 2331–2336.
Salmeen, I., & Palmer, G. (1968) *J. Chem. Phys. 48*, 2049–2052.
Schechter, E., & Saludjian, P. (1967) *Biopolymers 5*, 788–790.
Smith, D. W., & Williams, R. J. P. (1970) *Struct. Bonding (Berlin) 7*, 1–45.
Spaulding, L. D., Chang, C. C., Yu, N.-T., & Felton, R. H. (1975) *J. Am. Chem. Soc. 97*, 2517–2525.
Spiro, T. G., Stong, J. D., & Stein, P. (1979) *J. Am. Chem. Soc. 101*, 2648–2655.
Taylor, C. P. S. (1977) *Biochim. Biophys. Acta 491*, 137–149.
Walker, F. A., Reis, D., & Balke, V. L. (1984) *J. Am. Chem. Soc. 106*, 6888–6898.
Westhoff, P., Alt, J., Widger, W. R., Cramer, W. A., & Herrmann, R. G. (1985) *Plant Mol. Biol. 4*, 103–110.
Widger, W. R., Cramer, W. A., Hermodson, M., Meyer, D., & Gullifor, M. (1984a) *J. Biol. Chem. 259*, 3870–3876.
Widger, W. R., Cramer, W. A., Herrmann, R. G., & Trebst, A. (1984b) *Proc. Natl. Acad. Sci. U.S.A. 81*, 674–678.

Substrate Specificity of the Pea Chloroplast Glycolate Transporter†

Konrad T. Howitz* and Richard E. McCarty
Section of Biochemistry, Molecular and Cell Biology, Division of Biological Sciences, Cornell University, Ithaca, New York 14853
Received December 19, 1984

ABSTRACT: The transport of glycolic acid across the chloroplast envelope is a mediated process. Out of a number of metabolites assayed, only two or three carbon 2-hydroxymonocarboxylates significantly inhibited [^{14}C]glycolate uptake by intact pea chloroplasts. These compounds were found to be competitive inhibitors of glycolate uptake, with D-glycerate, D-lactate, and glyoxylate having K_i's approximately equal to the K_m for uninhibited glycolate uptake. L-Glycerate was less inhibitory than D-glycerate, and L-lactate did not appear to inhibit glycolate uptake. D-Glycerate, D-lactate, and glyoxylate caused countertransport of labeled glycolate, indicating that they are transportable substrates of the glycolate carrier. Glycolate and D-glycerate behaved similarly with respect to *N*-ethylmaleimide inhibition of their ability to increase the pH of the medium of a weakly buffered chloroplast suspension. An explanation is provided to resolve the apparent conflict of previous studies [Robinson, S. P. (1982) *Plant Physiol. 70*, 1032], with our conclusion that glycolate and D-glycerate, substrate and product, respectively, of the photorespiratory carbon cycle, are transported by the same carrier.

Glycolate is formed, in illuminated chloroplasts of C_3 plants, by the sequential action of ribulose-1,5-bisphosphate oxygenase and phosphoglycolate phosphatase. For every two glycolate molecules that leave the chloroplast, one glycerate, derived from glycolate by photorespiratory metabolism, enters it. One of the four carbons from the two glycolates is lost as CO_2. Glycerate is converted to 3-phosphoglycerate by the chloroplast glycerate kinase. As 3-phosphoglycerate, the three remaining carbons can reenter the Calvin cycle [see Ogren (1984) for a recent review].

Previous reports from our laboratory have shown the rate of glycolate transport across the envelope of intact pea chloroplasts to saturate with increasing glycolate concentration (Howitz & McCarty, 1983a, 1985). Transport was inhibited by pretreatment of the chloroplasts with *N*-ethylmaleimide (Howitz & McCarty, 1983a, 1985). These results indicated that the transport of glycolate across the chloroplast envelope is carrier mediated. Recently, we have developed multilayered silicon oil centrifugation techniques which have shortened the

†This work was supported by a research grant from the USDA-CRGO (8300670).

0006-2960/85/0424-3645$01.50/0